

Virtual Full-Duplex Wireless Communications with Zero-Interval Modulation and Sampling

Jianyu Wang, *Member, IEEE*, Wenchi Cheng, *Senior Member, IEEE*, Wei Zhang, *Fellow, IEEE*, and Hailin Zhang, *Member, IEEE*

Abstract—In this paper, we propose a virtual full-duplex (VFD) technique with zero-interval modulation and sampling (ZIMS), where two half-duplex (HD) transceivers can simultaneously transmit signals and each transceiver can effectively receive the desired information. In ZIMS-VFD, the transceiver inserts a zero-interval for each symbol in the transmit signal and provides self-interference (SI)-free intervals for itself. Meanwhile, it samples the receive signal in the provided SI-free intervals and restores the desired symbols. Based on orthogonal frequency division multiplexing (OFDM), we formulate the system model and show the transmit signal structure. Then, we give the transceiver design for single input single output (SISO) ZIMS-VFD and extend it to multiple input multiple output (MIMO) communications. Numerical results verify our theoretical analyses and show that ZIMS-VFD can effectively increase the capacity and approach the FD without SI.

Index Terms—Virtual full-duplex (VFD), orthogonal frequency division multiplexing (OFDM), zero-interval, modulation, sampling, multiple input multiple output (MIMO).

I. INTRODUCTION

FULL-duplex (FD), where transceivers can transmit and receive signals simultaneously in the same frequency-band, has gained substantial attention due to the potential to double the capacity of wireless communication networks [1]. The most critical challenge for FD is to cancel the self-interference (SI), which is the interference leaked from the local transmitter to the local receiver [2], [3]. In practice, SI is hard to be completely canceled because it is much stronger than the desired signals from other transceivers [4], [5]. To achieve FD, a series of self-interference cancellation (SIC) techniques are desired to be comprehensively utilized [6].

Based on the location where the SI is canceled, SIC techniques can be divided into propagation domain SIC, analog domain SIC, and digital domain SIC. Propagation domain SIC is the first step to cancel the SI. The authors of [7] used two transmit antennas whose distances from the receive antenna differ by half a wavelength. Thus, the SI signals can add destructively. Also, in [8], antenna design with resonant wavetraps has been used to improve electromagnetic isolation in a compact device. Moreover, in [9], an antenna isolation architecture based on electrical balance in hybrid junctions

has been proposed, which is based a single antenna and can be implemented on-chip.

After the propagation domain cancellation, the residual SI needs to be further canceled using a radio frequency (RF) or base-band analog canceller before the analog-to-digital converter (ADC). For examples, the authors of [10] presented a novel tapped delay line RF canceller with multiple non-uniform pre-weighted taps, which can not only cancel the SI from the direct transmit-to-receive antenna coupling but also the SI from reflection paths. Also, it is shown in [11] that the global optimal solution to the weights of the multi-tap RF canceller is given. Moreover, in [12], SI is first canceled by an integrated hybrid in the RF front-end, which can track the antenna impedance variations, and then canceled in the base-band analog domain based on the down-converted sampling of the transmit signal. In addition, taking nonlinear distortion into account, the authors of [13] combined self-adaptive RF cancellation with a shared-antenna architecture and achieved 40 dB SIC. The SIC in the propagation domain and analog domain guarantees that the weak desired signal can be sampled by ADC and not concealed in quantization noise [14].

After analog cancellation, SI needs to be further canceled in the digital domain. For examples, the authors of [15] proposed to use the digital domain copy of RF transmit signal to mitigate both the SI and transceiver impairments. Also, it is shown in [16] that the receive beamforming is done in the digital domain to mitigate SI. In addition, the authors of [17] considered RF imperfections and showed that the dominant SI in digital domain after antenna isolation and RF cancellation can be modeled through a widely linear transformation of the original transmit data. Based on the model, they proposed a widely linear digital SIC scheme. We can observe from above works that to cancel the strong SI, a series of complex works in the propagation domain, analog domain, and digital domain are desired to be done. Thus, the system complexity of FD is relatively high as compared with half-duplex (HD).

To avoid the complex SIC, a feasible way is virtual full-duplex (VFD). Two typical VFD techniques are VFD relaying and rapid on-off-division duplex (RODD). In VFD relaying, two or more HD relays are used to assist the transmission from the source to the destination. The relays are separated in space or time and alternately receive and forward. The inter-relay interferences (IRI) are much weaker than SI in FD. Thus, the source can transmit information in every time-slot and the spectrum efficiency loss of HD can be compensated. The authors of [18] proposed a VFD relaying scheme where the selected best relay forwards the packet while other relays

Jianyu Wang, Wenchi Cheng, and Hailin Zhang are with State Key Laboratory of Integrated Services Networks, Xidian University, Xi'an, 710071, China (e-mails: wangjianyu@xidian.edu.cn; wccheng@xidian.edu.cn; hlzhang@xidian.edu.cn).

Wei Zhang is with School of Electrical Engineering and Telecommunications, the University of New South Wales, Sydney, Australia (e-mails: w.zhang@unsw.edu.au).

attempt to decode the new packet. Taking into account the IRI, the overall outage probability is obtained in closed-form. Also, instead of avoiding or canceling IRI, in [19] IRI is considered as an additional source of energy to the relay and exploited for energy harvesting. In addition, VFD cooperative non-orthogonal multiple access (NOMA) is investigated in [20], where a relay selection algorithm with adaptive IRI management is proposed and the corresponding diversity-multiplexing tradeoff performance is analyzed based on a discrete Markov chain. However, VFD relaying technique focuses on relay channel with two or more relays, which cannot be extended to the point-to-point communications.

RODD is another VFD technique and can be used in point-to-point communications. The transceiver with RODD follows a random on-off mask to transmit and receives in the off-slots. Based on RODD, transceivers can transmit and receive simultaneously and achieve FD at the frame level. The authors of [21] proposed RODD and investigated the throughput. In [22], mutual broadcasting with RODD signaling is investigated and a practical algorithm for encoding and decoding the short messages is provided. Also, the hardware implementation of RODD has been shown in [23]. However, in RODD, SI leads to erasure-slots in the receive signal. The data corresponding to erasure-slots is lost during the transmission and needs to be restored based on channel coding. Additional bits are required to correct the data corresponding to erasure-slots, which results in the throughput reduction. To the best of our knowledge, it is currently unclear how to use HD transceivers to achieve point-to-point FD without losing the information of the signal with SI.

In this paper, we propose a point-to-point VFD communication technique with zero-interval modulation and sampling (ZIMS), which uses two HD transceivers to achieve FD communication. Specifically, a zero-interval is inserted for each symbol in the transmit signal of each transceiver to provide the corresponding SI-free interval for itself. Meanwhile, it samples the receive signal without SI in the provided SI-free interval and restores the desired symbol. Since ZIMS-VFD achieves FD with modulation and sampling, the hardware overheads associated with SIC, which usually include voluminous and power demanding components, can be reduced. In addition, as compared with RODD, where additional bits are required to restore the data of erasure-slots, ZIMS-VFD can restore the desired symbols from the samples in SI-free intervals without additional coding. Thus, ZIMS-VFD can achieve a higher capacity. Based on orthogonal frequency division multiplexing (OFDM), we formulate the system model and show the transmit signal structure. Then, we give the transceiver design for single input single output (SISO) ZIMS-VFD and extend it to multiple input multiple output (MIMO) communications. Moreover, numerical evaluations are conducted to verify our theoretical analyses.

The remainder of this paper is structured as follows. In Section II, we formulate the system model and show the transmit signal structure. In Section III, we give the transceiver design for SISO ZIMS-VFD. In Section IV, SISO ZIMS-VFD is extended to MIMO communications. Numerical evaluations are conducted in Section V. We conclude in Section VI.

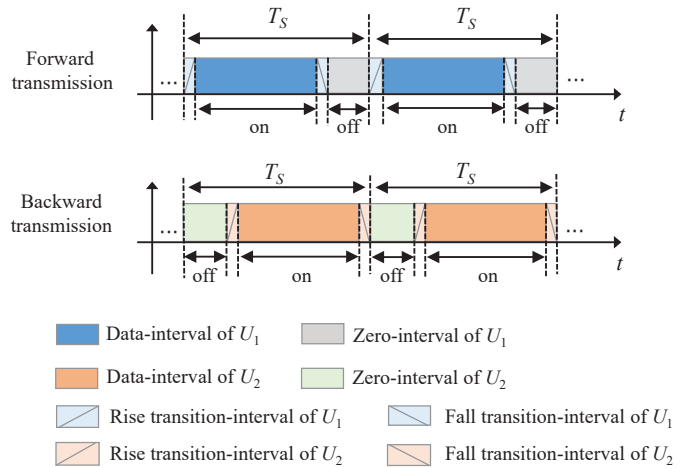


Fig. 1. Transmit signal structure of ZIMS-VFD.

II. SYSTEM MODEL AND TRANSMIT SIGNAL STRUCTURE FOR ZIMS-VFD

We consider a point-to-point communication, where two HD transceivers, denoted by U_1 and U_2 , exchange information simultaneously in the same frequency-band. The numbers of transmit antennas and receive antennas of U_i are $K_{T,i}$ and $K_{R,i}$, respectively ($i \in \{1, 2\}$). We assume that the transmit signal of each transceiver is based on orthogonal frequency division multiplexing (OFDM) with $2N$ subcarriers. The frequency corresponding to the n -th subcarrier, denoted by f_n , is $f_n = f_c + n\Delta f$, where Δf is the bandwidth of each subcarrier and f_c is the center frequency ($n \in \{-N + 1, \dots, 0, \dots, N\}$). It is assumed that U_1 and U_2 are well synchronized with techniques such as global positioning system (GPS) [21], [22] and MIMO cable [23].

The transmit signal structure of ZIMS-VFD is shown in Fig. 1, where the forward transmission (from U_1 to U_2) and the backward transmission (from U_2 to U_1) are overlapped in the time domain. Each transceiver uses RF switches to insert a zero-interval for each OFDM symbol period in the transmit signal. In practice, RF switching is not instantaneous and results in transitions, including rise transitions and fall transitions. Rise transitions are the switching periods from off to on. Fall transitions are the switching periods from on to off. We assume both rise transitions and fall transitions are less than a value δ . The OFDM symbol period of U_i , denoted by T_S , is designed to have a data-interval, denoted by $T_D = 1/\Delta f$, a rise transition-interval, denoted by T_R , a fall transition-interval, denoted by T_F , and a zero-interval, denoted by T_Z . The expression of T_S is given by

$$T_S = T_D + T_R + T_F + T_Z. \quad (1)$$

We set $T_R = T_F = \delta$ to guarantee transitions are always within rise transition-intervals or fall transition-intervals and have no impact on zero-intervals and data-intervals. In the zero-interval, the transmit chain of each antenna is off, which can provide an SI-free interval for local receivers. In the SI-free interval, the receive chain of each antenna turns on and samples the signal without SI. In the SI interval, the receive

chain of each antenna turns off and shields the SI. Also, as shown in Fig. 1, the transmit signal structures of U_1 and U_2 are different. The data-interval of U_1 is before its zero-interval and the data-interval of U_2 is after its zero-interval. The structure difference aims to guarantee that the desired signals are non-zero in the SI-free interval. Note that if $T_R + T_F + T_Z > T_D$, more than half of the transmit signal carries no information and ZIMS-VFD brings no symbol rate gain as compared to traditional HD. Thus, to guarantee a relatively high symbol rate, T_D needs to satisfy

$$T_D > T_Z + 2\delta. \quad (2)$$

The channel model we employ is block fading. We denote by $\delta(t)$ the impulse function and $L_{i,k,p,q}$ the number of paths corresponding to the channel from the p -th transmit antenna of U_i to the q -th receive antenna of U_k ($k \in \{1, 2\}$, $p \in \{1, 2, \dots, K_{T,i}\}$, and $q \in \{1, 2, \dots, K_{R,k}\}$). Then, based on the channel model, we can write the impulse response of the channel from the p -th antenna of U_i to the q -th antenna of U_k as follows [24], [25]:

$$h_{i,k,p,q}(t) = \sum_{l=1}^{L_{i,k,p,q}} a_{i,k,p,q}^l \delta(t - \tau_{i,k,p,q}^l), \quad (3)$$

where $a_{i,k,p,q}^l$ and $\tau_{i,k,p,q}^l$ denote the amplitude gain and the delay of the l -th path, respectively.

If T_Z is less than the maximum delay spread of SI channels, each transceiver cannot provide SI-free intervals for the local receiver since they are covered by the local transmit signal. On the other hand, if T_Z is less than the maximum delay spread of channels from U_1 (U_2) to U_2 (U_1), inter symbol interference (ISI) occurs. Thus, to avoid ISI and provide SI-free intervals for the local receiver, T_Z needs to satisfy

$$T_Z > \tau_{\max}, \quad (4)$$

where $\tau_{\max} = \max_{i,k,p,q,l} \{\tau_{i,k,p,q}^l\} - \min_{i,k,p,q,l} \{\tau_{i,k,p,q}^l\}$. The inserted zero-intervals in the transmit signal are designed to not only help avoid SI but also inter symbol interference (ISI). Thus, to guarantee the spectrum efficiency, we don't insert additional cyclic prefixes (CPs) into the transmit signal. In addition, we set the bandwidth of each subcarrier to satisfy $\Delta f < 1/\tau_{\max}$, which is equivalent to

$$T_D > \tau_{\max}, \quad (5)$$

such that each subchannel is flat.

III. TRANSCIVER DESIGN FOR SISO ZIMS-VFD

In this section, we first introduce the transceiver design for SISO ZIMS-VFD. The extension of ZIMS-VFD to MIMO communications is discussed in Section IV. We consider a block with M OFDM symbol periods. The transmit symbol corresponding to the n -th subcarrier of U_i in the m -th OFDM symbol period is denoted by $X_i^{n,m}$. Then, the transmit signal

of U_1 in the m -th OFDM symbol period, denoted by $x_1^m(t)$, can be given by

$$x_1^m(t) = \begin{cases} R_1^m(t), & mT_S \leq t < mT_S + \delta; \\ \sum_{n=-N+1}^N X_1^{n,m} e^{j2\pi f_n t}, & mT_S + \delta \leq t < mT_S + \delta + T_D; \\ F_1^m(t), & mT_S + \delta + T_D \leq t < (m+1)T_S - T_Z; \\ 0, & (m+1)T_S - T_Z \leq t < (m+1)T_S, \end{cases} \quad (6)$$

where $R_1^m(t)$ and $F_1^m(t)$ are rise and fall transitions in the m -th OFDM symbol period of U_1 . Similarly, the transmit signal of U_2 in the m -th OFDM symbol period, denoted by $x_2^m(t)$, can be given by

$$x_2^m(t) = \begin{cases} 0, & mT_S \leq t < mT_S + T_Z; \\ R_2^m(t), & mT_S + T_Z \leq t < mT_S + T_Z + \delta; \\ \sum_{n=-N+1}^N X_2^{n,m} e^{j2\pi f_n t}, & mT_S + T_Z + \delta \leq t < (m+1)T_S - \delta; \\ F_2^m(t), & (m+1)T_S - \delta \leq t < (m+1)T_S, \end{cases} \quad (7)$$

where $R_2^m(t)$ and $F_2^m(t)$ are rise and fall transitions in the m -th OFDM symbol period of U_2 . Based on (3), (6), and (7), the signal at the receive antenna of U_i , denoted by $y_i(t)$, can be given by

$$y_i(t) = \underbrace{\sum_{m=1}^M x_i^m(t) * h_{i,i}(t)}_{\text{SI}} + \underbrace{\sum_{m=1}^M x_{3-i}^m(t) * h_{3-i,i}(t)}_{\text{Desired signal}} + z_i(t), \quad (8)$$

where $*$ denotes the convolution and $z_i(t)$ denotes the noise of U_i . Since SISO system is considered, the antenna subscripts p and q are omitted in this section. Then, the receive signal given by (8) is processed in SI-free intervals to restore the desired symbols. The details are shown in the next two subsections.

A. Candidate Intervals Determination

To avoid SI, the receive chain of each transceiver turns on in SI-free intervals and turns off in SI intervals, as shown in Fig. 2. RF switching also results in transitions in the receive chain. Similar to the transmit chain, we assume that they are less than δ . To restore the desired symbols, (8) needs to be sampled in the intervals where the SI is zero, the transitions of the receive chain are zero, and the desired signal is within the data-interval. We call this kind of intervals candidate intervals and determine them in the following.

To determine the candidate intervals, we first investigate the SI-free intervals, where the SI is zero, for each transceiver. Based on (3), (6), (7), and (8), the m -th SI-free intervals of U_1 and U_2 , denoted by $\mathcal{T}_{F,1}^m$ and $\mathcal{T}_{F,2}^m$, can be expressed as

$$\mathcal{T}_{F,1}^m = \{t | (m+1)T_S - T_Z + \tau_{1,1}^{\max} \leq t < (m+1)T_S + \tau_{1,1}^{\min}\} \quad (9)$$

and

$$\mathcal{T}_{F,2}^m = \{t | mT_S + \tau_{2,2}^{\max} \leq t < mT_S + T_Z + \tau_{2,2}^{\min}\}, \quad (10)$$

respectively, where $\tau_{i,k}^{\max} = \max_l \{\tau_{i,k}^l\}$ and $\tau_{i,k}^{\min} = \min_l \{\tau_{i,k}^l\}$. The RF switches corresponding to the receive chains of U_1

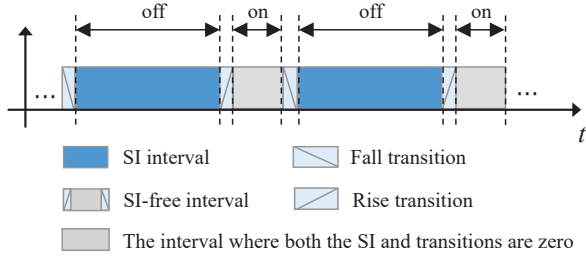


Fig. 2. RF switching in the receive chain of ZIMS-VFD.

and U_2 start to turn on at the left ends of $\mathcal{T}_{F,1}^m$ and $\mathcal{T}_{F,2}^m$, that is, $(m+1)T_S - T_Z + \tau_{1,1}^{\max}$ and $mT_S + \tau_{2,2}^{\max}$, respectively. Before $(m+1)T_S - T_Z + \tau_{1,1}^{\max}$ and $mT_S + \tau_{2,2}^{\max}$, the receive chains of U_1 and U_2 are in the off state, such that they can shield the SI before the left ends of $\mathcal{T}_{F,1}^m$ and $\mathcal{T}_{F,2}^m$. After a period of time δ , transitions disappear and the receive chains will be in the on state. On the other hand, the RF switches corresponding to the receive chains of U_1 and U_2 start to turn off at $(m+1)T_S + \tau_{1,1}^{\min} - \delta$ and $mT_S + T_Z + \tau_{2,2}^{\min} - \delta$, respectively. After a period of time δ , the receive chains will be in the off state and transitions disappear before the right ends of $\mathcal{T}_{F,1}^m$ and $\mathcal{T}_{F,2}^m$. Thus, the SI after the right ends of $\mathcal{T}_{F,1}^m$ and $\mathcal{T}_{F,2}^m$ can be shielded. We denote by $\mathcal{T}_{FT,i}^m$ the intervals where both the SI and receive transitions of U_i are zero. Then, $\mathcal{T}_{FT,1}^m$ and $\mathcal{T}_{FT,2}^m$ can be expressed as

$$\mathcal{T}_{FT,1}^m = \{t | (m+1)T_S - T_Z + \tau_{1,1}^{\max} + \delta \leq t < (m+1)T_S + \tau_{1,1}^{\min} - \delta\} \quad (11)$$

and

$$\mathcal{T}_{FT,2}^m = \{t | mT_S + \tau_{2,2}^{\max} + \delta \leq t < mT_S + T_Z + \tau_{2,2}^{\min} - \delta\}, \quad (12)$$

respectively. Next we investigate the data-interval corresponding to the desired signal of U_i . Based on (3), (6), (7), and (8), the m -th data-intervals corresponding to the desired signals of U_1 and U_2 , denoted by $\mathcal{T}_{D,1}^m$ and $\mathcal{T}_{D,2}^m$, can be given by

$$\mathcal{T}_{D,1}^m = \{t | mT_S + T_Z + \delta + \tau_{2,1}^{\min} \leq t < (m+1)T_S - \delta + \tau_{2,1}^{\max}\} \quad (13)$$

and

$$\mathcal{T}_{D,2}^m = \{t | mT_S + \delta + \tau_{1,2}^{\min} \leq t < mT_S + \delta + T_D + \tau_{1,2}^{\max}\}, \quad (14)$$

respectively.

We denote by $\mathcal{T}_{C,i}^m = \mathcal{T}_{FT,i}^m \cap \mathcal{T}_{D,i}^m$ the m -th candidate interval of U_i , where the desired signal of U_i is within the data-interval and the SI of U_i is zero. Then, $\mathcal{T}_{C,i}^m$ can be expressed as

$$\mathcal{T}_{C,i}^m = \{t | \chi_{L,i}^m \leq t \leq \chi_{U,i}^m\} \quad (15)$$

with

$$\chi_{U,1}^m = \min \{(m+1)T_S + \tau_{1,1}^{\min} - \delta, (m+1)T_S - \delta + \tau_{2,1}^{\max}\}, \quad (16)$$

$$\chi_{L,1}^m = \max \{(m+1)T_S - T_Z + \tau_{1,1}^{\max} + \delta, mT_S + T_Z + \delta + \tau_{2,1}^{\min}\}, \quad (17)$$

$$\chi_{U,2}^m = \min \{mT_S + T_Z + \tau_{2,2}^{\min} - \delta, mT_S + \delta + T_D + \tau_{1,2}^{\max}\}, \quad (18)$$

and

$$\chi_{L,2}^m = \max \{mT_S + \tau_{2,2}^{\max} + \delta, mT_S + \delta + \tau_{1,2}^{\min}\}. \quad (19)$$

We denote by $T_{C,i}^m = \chi_{U,i}^m - \chi_{L,i}^m$ the length of the m -th candidate interval of U_i and have the following theorem.

Theorem 1: If T_Z satisfies

$$T_Z > 2\delta + \tau_{\max}, \quad (20)$$

$T_{C,i}^m > 0$ can always be guaranteed.

Proof 3.1: Please refer to Appendix A.

Remarks on Theorem 1: Theorem 1 shows that if (20) is satisfied, the transmit signal design, that is, the data-interval of U_1 is before its zero-interval and the data-interval of U_2 is after its zero-interval, can provide a candidate interval with a length larger than zero for each desired OFDM symbol. Theorem 1 proves the existence of each candidate interval and the feasibility of ZIMS-VFD to simultaneously avoid the SI and sample the desired signal in data-interval. Combining (2), (4), (5), and (20), we can obtain the condition that T_Z and T_D need to satisfy:

$$\tau_{\max} + 2\delta < T_Z < T_D - 2\delta. \quad (21)$$

B. Sampling and Desired Symbols Restoration

If (21) holds, candidate intervals exist. In the m -th candidate interval of U_i , the SI is zero and the signal at the receive antenna of U_i is

$$y_i(t) = \sum_{n=-N+1}^N H_{3-i,i}^n X_{3-i}^{n,m} e^{j2\pi f_n t} + z_i(t), \quad (22)$$

where $H_{i,k}^n$ denotes the frequency-domain channel gain with the expression of

$$H_{i,k}^n = \sum_{l=1}^{L_{i,k}} a_{i,k}^l e^{-j2\pi f_n \tau_{i,k}^l}. \quad (23)$$

Then, $y_i(t)$ is sampled G times in $\mathcal{T}_{C,i}^m$ ($G > 2N$). We denote by $\hat{t}_i^{v,m}$ the v -th sampling time in $\mathcal{T}_{C,i}^m$. The expression of $\hat{t}_i^{v,m}$ can be expressed as

$$\hat{t}_i^{v,m} = \chi_{L,i}^m + \frac{T_{C,i}^m v}{2N}. \quad (24)$$

Based on the samples in each $\mathcal{T}_{C,i}^m$, we can obtain the receive signal in the digital domain. The sampling sequence in $\mathcal{T}_{C,i}^m$ can be derived based on (22) and (23) as follows:

$$\mathbf{Y}_{i,m} = \mathbf{V}_{i,m} \mathbf{H}_{3-i,i} \mathbf{X}_{3-i,m} + \mathbf{Z}_{i,m}. \quad (25)$$

In (25),

$$\mathbf{Y}_{i,m} = [Y_i^{1,m}, Y_i^{2,m}, \dots, Y_i^{G,m}]^T, \quad (26)$$

where the v -th entry is the value of the v -th sampling point,

$$\mathbf{X}_{3-i,m} = [X_{3-i}^{-N+1,m}, X_{3-i}^{-N+2,m}, \dots, X_{3-i}^{N,m}]^T \quad (27)$$

is the transmit symbol vector of U_{3-i} , where $(\cdot)^T$ denotes the transpose operation,

$$\mathbf{H}_{3-i,i} = \text{diag} [H_{3-i,i}^{-N+1}, H_{3-i,i}^{-N+2}, \dots, H_{3-i,i}^N] \quad (28)$$

$$\mathbf{V}_{i,m} = \begin{bmatrix} e^{j2\pi f_{-N+1}\hat{t}_i^{1,m}} & e^{j2\pi f_{-N+2}\hat{t}_i^{1,m}} & \dots & e^{j2\pi f_N\hat{t}_i^{1,m}} \\ e^{j2\pi f_{-N+1}\hat{t}_i^{2,m}} & e^{j2\pi f_{-N+2}\hat{t}_i^{2,m}} & \dots & e^{j2\pi f_N\hat{t}_i^{2,m}} \\ \vdots & \vdots & \ddots & \vdots \\ e^{j2\pi f_{-N+1}\hat{t}_i^{G,m}} & e^{j2\pi f_{-N+2}\hat{t}_i^{G,m}} & \dots & e^{j2\pi f_N\hat{t}_i^{G,m}} \end{bmatrix} \quad (29)$$

$$C_S = \frac{\Delta f}{(1+\alpha)M} \sum_{m=1}^M \left[\log_2 \det \left(\mathbf{I}_G + \frac{\mathbf{V}_{1,m}\mathbf{H}_{2,1}\mathbf{R}_{2,m}\mathbf{H}_{2,1}^H\mathbf{V}_{1,m}^H}{\sigma_0^2} \right) + \log_2 \det \left(\mathbf{I}_G + \frac{\mathbf{V}_{2,m}\mathbf{H}_{1,2}\mathbf{R}_{1,m}\mathbf{H}_{1,2}^H\mathbf{V}_{2,m}^H}{\sigma_0^2} \right) \right] \quad (30)$$

is the channel matrix from U_{3-i} to U_i ,

$$\mathbf{Z}_{i,m} = \left[\bar{z}_i(\hat{t}_i^{1,m}), \bar{z}_i(\hat{t}_i^{2,m}), \dots, \bar{z}_i(\hat{t}_i^{G,m}) \right]^T \quad (31)$$

is the noise vector, where each entry is assumed to follow $\mathcal{CN}(0, \sigma_0^2)$ with σ_0^2 representing the variance of the noise, $\mathbf{V}_{i,m} \in \mathbb{C}^{G \times 2N}$ is related to the sampling times and subcarrier frequencies, which is given by (29) at the top of this page. In this paper we call $\mathbf{V}_{i,m}$ sampling matrix. It can be observed from (25) that the equivalent channel matrix is $\mathbf{V}_{i,m}\mathbf{H}_{3-i,i}$. We have the following theorem for $\mathbf{V}_{i,m}\mathbf{H}_{3-i,i}$.

Theorem 2: $\text{Rank}(\mathbf{V}_{i,m}\mathbf{H}_{3-i,i}) = 2N$, where $\text{Rank}(\cdot)$ is the operation of taking the rank.

Proof 3.2: Please refer to Appendix B.

Remarks on Theorem 2: Theorem 2 implies that $\mathbf{V}_{i,m}\mathbf{H}_{3-i,i}$ is full-rank and can be transformed into $2N$ parallel subchannels. Thus, sampling in candidate intervals can achieve the same freedom degrees as conventional OFDM, where the sampling points are uniformly distributed in the entire OFDM symbol period.

In ZIMS-VFD, the sampling points are not uniformly distributed in the entire OFDM symbol period. Thus, it is difficult to directly restore $\mathbf{X}_{3-i,m}$ with discrete Fourier transform (DFT). We can consider $\mathbf{Y}_{i,m}$ as an output signal of a multiple input multiple output (MIMO) system. Based on (25), the sum capacity of SISO ZIMS-VFD can be given by (30). In (30), \mathbf{I}_G is a $G \times G$ identity matrix, $\mathbf{R}_{3-i,m} = \mathbb{E}\{\mathbf{X}_{3-i,m}\mathbf{X}_{3-i,m}^H\}$, where $\mathbb{E}\{\cdot\}$ represents the operation of taking expectation and the n -th main diagonal element is transmit power of the n -th subcarrier, and $\alpha = (T_Z + 2\delta)/T_D$.

Singular value decomposition (SVD) based pre-coding and pre-decoding can be used to restore the desired symbols and achieve the capacity given by (30) [24]. The singular value decomposition (SVD) of $\mathbf{V}_{i,m}\mathbf{H}_{3-i,i}$ can be given by

$$\mathbf{V}_{i,m}\mathbf{H}_{3-i,i} = \tilde{\mathbf{U}}_{i,m}\mathbf{S}_{i,m}\hat{\mathbf{U}}_{i,m}^H, \quad (32)$$

where $\tilde{\mathbf{U}}_{i,m} \in \mathbb{C}^{G \times G}$ and $\hat{\mathbf{U}}_{i,m} \in \mathbb{C}^{2N \times 2N}$ are two unitary matrices corresponding to $\mathbf{V}_{i,m}\mathbf{H}_{3-i,i}$, $(\cdot)^H$ denotes the conjugate transpose operation, and $\mathbf{S}_{i,m} \in \mathbb{C}^{G \times 2N}$ is the matrix with main diagonal entries equaling to the singular values of $\mathbf{V}_{i,m}\mathbf{H}_{3-i,i}$ and other entries equaling to zero. With the pre-coding of $\mathbf{X}_{3-i,m} = \hat{\mathbf{U}}_{i,m}\tilde{\mathbf{X}}_{3-i,m}$ and the pre-decoding of $\tilde{\mathbf{Y}}_{i,m} = \tilde{\mathbf{U}}_{i,m}^H\mathbf{Y}_{i,m}$, (25) can be converted into multiple parallel SISO transmissions:

$$\tilde{Y}_i^{\tilde{k},m} = \sqrt{\lambda_i^{\tilde{k},m}} \tilde{X}_{3-i}^{\tilde{k},m} + \tilde{Z}_i^{\tilde{k},m}, \quad \tilde{k} = 1, 2, \dots, 2N. \quad (33)$$

In (33), $\tilde{Y}_i^{\tilde{k},m}$ is the \tilde{k} -th entry of $\tilde{\mathbf{Y}}_{i,m}$, $\sqrt{\lambda_i^{\tilde{k},m}}$ is the \tilde{k} -th singular value of $\mathbf{V}_{i,m}\mathbf{H}_{3-i,i}$, $\tilde{X}_{3-i}^{\tilde{k},m}$ is the \tilde{k} -th entry of $\tilde{\mathbf{X}}_{3-i,m}$, whose average power can be given by $\mathbb{E}\{|\tilde{X}_{3-i}^{\tilde{k},m}|^2\} = P_{3-i}^{\tilde{k}}$, and $\tilde{Z}_i^{\tilde{k},m}$ is the \tilde{k} -th entry of $\tilde{\mathbf{U}}_{i,m}^H\mathbf{Z}_{i,m}$. Also, $P_i^{\tilde{k}}$ satisfies $\sum_{\tilde{k}=1}^{2N} P_i^{\tilde{k}} \leq \bar{P}_i$, where \bar{P}_i denotes the power constraint for U_i . Then, the estimation for $\tilde{X}_{3-i}^{\tilde{k},m}$, denoted by $\hat{X}_{3-i}^{\tilde{k},m}$, can be expressed as follows:

$$\hat{X}_{3-i}^{\tilde{k},m} = \arg \min_{X \in \mathbb{X}_{3-i}} \left| \frac{\tilde{Y}_i^{\tilde{k},m}}{\sqrt{\lambda_i^{\tilde{k},m}}} - X \right|^2, \quad (34)$$

where \mathbb{X}_{3-i} is the constellation that defines the transmit symbols of U_{3-i} . MIMO detection methods such as zero-forcing (ZF) detection, minimum mean square error (MMSE) detection, and MMSE with successive interference cancellation (SIC) can also be used to restore desired symbols [24], [26]. We omit them for brevity here. Based on (33), the signal to noise ratio (SNR) corresponding to the k -th parallel channel of U_i , denoted by $\gamma_i^{\tilde{k},m}$, can be given by

$$\gamma_i^{\tilde{k},m} = \frac{P_{3-i}^{\tilde{k}}\lambda_i^{\tilde{k},m}}{\sigma_0^2}. \quad (35)$$

If quadrature phase shift keying (QPSK) is used, the bit error rate (BER) corresponding to the k -th parallel channel of U_i , denoted by $p_{b,i}^{\tilde{k},m}$, can be given by [27]

$$p_{b,i}^{\tilde{k},m} = Q\left(\sqrt{\gamma_i^{\tilde{k},m}}\right). \quad (36)$$

The value of α , which depends on the value of T_Z , has significant impacts on the singular values of the equivalent channel. If α is small and the resulting $T_{C,i}$ is short, we can obtain a high symbol rate, which is $\Delta f/(1+\alpha)$ in (30). However, in this case, some values of $\lambda_i^{1,m}, \dots, \lambda_i^{2N,m}$ are small, that is, some subchannels are weak, since the samples are close, which results in the low capacity and high BER for the corresponding weak subchannels. On the other hand, if T_Z is large and the resulting $T_{C,i}$ is long, the values of $\lambda_i^{1,m}, \dots, \lambda_i^{2N,m}$ are uniform, which results in fewer weak subchannels. However, the large value of α results in a relatively low symbol rate. Thus, α not only affects the symbol rate but also the equivalent channel. The optimal α can be numerically found with one-dimensional search methods such as golden section and Fibonacci search [28].

$$C_S^{\text{MIMO}} = \frac{\Delta f}{(1+\alpha)M} \sum_{m=1}^M \left[\log_2 \det \left(\mathbf{I}_{K_{R,1}G} + \frac{\mathbf{V}_{1,m}^{\text{MIMO}} \mathbf{R}_{2,m}^{\text{MIMO}} (\mathbf{V}_{1,m}^{\text{MIMO}})^H}{\sigma_0^2} \right) + \log_2 \det \left(\mathbf{I}_{K_{R,2}G} + \frac{\mathbf{V}_{2,m}^{\text{MIMO}} \mathbf{R}_{1,m}^{\text{MIMO}} (\mathbf{V}_{2,m}^{\text{MIMO}})^H}{\sigma_0^2} \right) \right] \quad (37)$$

IV. MIMO ZIMS-VFD

In this section, we discuss how to extend the SISO ZIMS-VFD to MIMO communications.

If $\tau_{i,j}^{\max}$ and $\tau_{i,j}^{\min}$ in Section III are replaced with $\tau_{i,k}^{\max} = \max_{l,p,q} \{\tau_{i,k,p,q}^l\}$ and $\tau_{i,k}^{\min} = \min_{l,p,q} \{\tau_{i,k,p,q}^l\}$, respectively, (11)-(21) also hold for MIMO ZIMS-VFD. Therefore, candidate intervals determination, receiver switch control, and sampling are similar to those in SISO ZIMS-VFD. Next we analyze the symbol restoration for MIMO ZIMS-VFD. We denote by $\mathbf{X}_{i,p}^m \in \mathbb{C}^{2N \times 1}$ the transmit symbol vector corresponding to the p -th transmit antenna of U_i in the m -th OFDM symbol period, $\mathbf{Y}_{i,q}^m \in \mathbb{C}^{2N \times 1}$ the sampling sequence corresponding to the q -th receive antenna of U_i in the m -th candidate interval, $\mathbf{H}_{i,k}^{p,q} \in \mathbb{C}^{2N \times 2N}$ the frequency-domain channel matrix from the p -th transmit antenna of U_i to the q -th receive antenna of U_k . Then, the receive signal vector of U_i , denoted by $\mathbf{Y}_{i,m}^{\text{MIMO}} \in \mathbb{C}^{K_{R,i}G \times 1}$, can be given by

$$\mathbf{Y}_{i,m}^{\text{MIMO}} = \mathbf{V}_{i,m}^{\text{MIMO}} \mathbf{X}_{3-i,m}^{\text{MIMO}} + \mathbf{Z}_{i,m}^{\text{MIMO}}. \quad (38)$$

In (38), $\mathbf{Y}_{i,m}^{\text{MIMO}}$ is given by $\mathbf{Y}_{i,m}^{\text{MIMO}} = [\mathbf{Y}_{i,1}^m, \dots, \mathbf{Y}_{i,K_{R,i}}^m]^T$, $\mathbf{X}_{3-i,m}^{\text{MIMO}} \in \mathbb{C}^{2K_{T,3-i}N \times 1}$ is the transmit symbol vector of U_{3-i} and given by $\mathbf{X}_{3-i,m}^{\text{MIMO}} = [\mathbf{X}_{3-i,1}^m, \dots, \mathbf{X}_{3-i,K_{T,3-i}}^m]^T$, $\mathbf{V}_{i,m}^{\text{MIMO}} \in \mathbb{C}^{K_{R,i}G \times 2K_{T,3-i}N}$ is the equivalent channel matrix given by

$$\mathbf{V}_{i,m}^{\text{MIMO}} = \begin{bmatrix} \mathbf{V}_{i,m} \mathbf{H}_{3-i,i}^{1,1} & \cdots & \mathbf{V}_{i,m} \mathbf{H}_{3-i,i}^{K_{T,3-i},1} \\ \vdots & \ddots & \vdots \\ \mathbf{V}_{i,m} \mathbf{H}_{3-i,i}^{1,K_{R,i}} & \cdots & \mathbf{V}_{i,m} \mathbf{H}_{3-i,i}^{K_{T,3-i},K_{R,i}} \end{bmatrix}, \quad (39)$$

where $\mathbf{V}_{i,m} \mathbf{H}_{3-i,i}^{p,q}$ is the equivalent channel matrix from the p -th transmit antenna of U_{3-i} to the q -th receive antenna of U_i . We have the following theorem for $\mathbf{V}_{i,m}^{\text{MIMO}}$.

Theorem 3: $\text{Rank}(\mathbf{V}_{i,m}^{\text{MIMO}}) = \text{Rank}(\mathbf{H}_{3-i,i}^{\text{MIMO}})$, where

$$\mathbf{H}_{3-i,i}^{\text{MIMO}} = \begin{bmatrix} \mathbf{H}_{3-i,i}^{1,1} & \cdots & \mathbf{H}_{3-i,i}^{K_{T,3-i},1} \\ \vdots & \ddots & \vdots \\ \mathbf{H}_{3-i,i}^{1,K_{R,i}} & \cdots & \mathbf{H}_{3-i,i}^{K_{T,3-i},K_{R,i}} \end{bmatrix}. \quad (40)$$

Proof 4.1: Please refer to Appendix C.

Remarks on Theorem 3: Theorem 3 shows that $\mathbf{V}_{i,m}$ has no impact on the rank of $\mathbf{V}_{i,m}^{\text{MIMO}}$, which implies that the sampling in candidate intervals has no impact on the rank of equivalent MIMO channel, and can achieve the same freedom degrees as conventional MIMO-OFDM communications.

Based on (38), the sum capacity of MIMO ZIMS-VFD can be given by (37). In (37), $\mathbf{I}_{K_{R,i}G}$ is a $K_{R,i}G \times K_{R,i}G$ identity matrix, $\mathbf{R}_{3-i,m}^{\text{MIMO}} = \mathbb{E}\{\mathbf{X}_{3-i,m}^{\text{MIMO}} (\mathbf{X}_{3-i,m}^{\text{MIMO}})^H\}$. Then, similar to single-antenna case, based on the SVD of $\mathbf{V}_{i,m}^{\text{MIMO}}$, (37) can be achieved and the desired symbols can be restored. MIMO

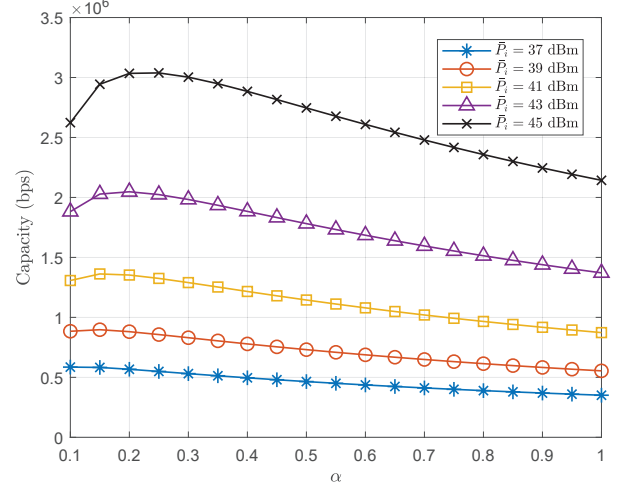


Fig. 3. The capacity of SISO ZIMS-VFD with different values of α and \bar{P}_i .

detection methods such as ZF detection, MMSE detection, and MMSE-SIC detection can also be used to restore the desired symbols [24], [26].

V. NUMERICAL EVALUATIONS

In this section, numerical evaluations are conducted to show the performance of ZIMS-VFD. The general parameters in evaluations are as follows. The maximum delay spread is set to $\tau_{\max} = 100$ ns, the upper-bound of transitions is set to $\delta = 1.9 \mu\text{s}$ [29], [30], the central frequency is set to $f_c = 2.4$ GHz, the bandwidth is set to $B = 20$ MHz, the channel gains of SI channels follow $H_{i,i}^{p,q} \sim \mathcal{CN}(0, 1)$, the channel gains of desired channels follow $H_{3-i,i}^{p,q} \sim \mathcal{CN}(0, 10^{-10})$, the noise power is set to $\sigma_0^2 = N_0 B$ where N_0 is set to -150 dBm/Hz, the number of samples in each candidate interval is $2N$.

Figure 3 shows the capacity of SISO ZIMS-VFD with different values of α and \bar{P}_i , where the number of subcarriers is set to $2N = 2048$ and the power constraint for each transceiver is set to $\bar{P}_i = 37$ dBm, $\bar{P}_i = 39$ dBm, $\bar{P}_i = 41$ dBm, $\bar{P}_i = 43$ dBm, and $\bar{P}_i = 45$ dBm. The transmit power of each transceiver is averagely allocated to subcarriers and the value of α ranges from 0.1 to 1. It can be known from Fig. 3 that if the power constraint is relatively small, for example, $\bar{P}_i = 37$ dBm, the capacity of SISO ZIMS-VFD monotonically decreases as α increases. If the power constraint is relatively large, for example, $\bar{P}_i = 41$ dBm, the capacity of SISO ZIMS-VFD doesn't monotonically varies as α increases. Therefore, in low power region, the value of α needs to be chosen as small as possible. In high power region, the minimum α may not be optimal. The optimal α can be numerically found with one-dimensional search methods such as golden section search and Fibonacci search [28].

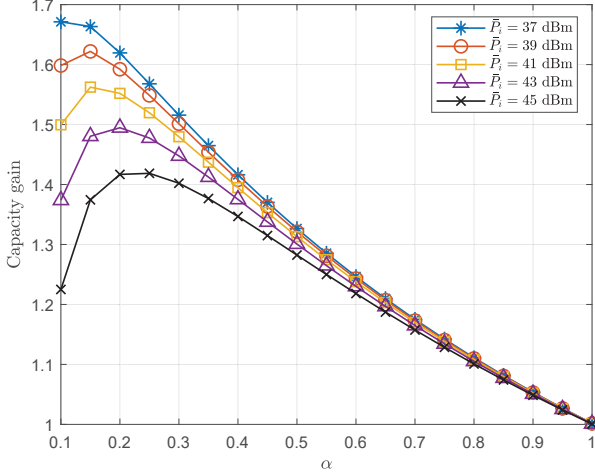


Fig. 4. The capacity gain of SISO ZIMS-VFD over SISO OFDM-HD with different values of α and \bar{P}_i .

Figure 4 shows the capacity gain of SISO ZIMS-VFD over conventional SISO OFDM-HD, which refers to the ratio of the capacity of SISO ZIMS-VFD to the capacity of conventional SISO OFDM-HD, with different values of α and \bar{P}_i . The CP length of SISO OFDM-HD is set to $2\tau_{\max}$. The number of subcarriers, power constraint for each transceiver, power allocation and the range of α are the same as Fig. 3. We can observe from Fig. 4 that the capacity gain is larger than 1, which implies that SISO ZIMS-VFD outperforms conventional SISO OFDM-HD in capacity. Also, the capacity gain decreases as \bar{P}_i increases, which implies that SISO ZIMS-VFD has the better performance gain in low-power region. In addition, the optimal α to maximize the capacity gain monotonically increases as \bar{P}_i increases. Moreover, we can see that the capacity gain is approximately equal to 1 if $\alpha = 1$, that is, $T_Z = T_D - 2\delta$. This is because the forward transmission and the backward transmission of ZIMS-VFD are completely separated due to the relatively long zero-interval.

Figure 5 shows the capacity gain of SISO ZIMS-VFD over SISO OFDM-HD with different values of α and $2N$. The CP length of SISO OFDM-HD is set to $2\tau_{\max}$. The number of subcarriers is set to $2N = 256$, $2N = 512$, $2N = 1024$, and $2N = 2048$. The power constraint for each transceiver is 40 dBm and the power is averagely allocated for subcarriers. We set the range of α is from 0.3 to 1. It can be known from Fig. 5 that the capacity gain monotonically increases as the value of $2N$ increases, which implies that SISO ZIMS-VFD is suitable for OFDM transmission with a large number of subcarriers. Also, we can observe that if the subcarrier number is relatively large, for example, $2N = 2048$, the capacity of SISO ZIMS-VFD monotonically decreases as α increases. If the subcarrier number is relatively small, for example, $2N = 512$, the capacity of SISO ZIMS-VFD doesn't monotonically varies as $2N$ increases. Therefore, if the number of subcarriers is large, the value of α needs to be chosen as small as possible. Otherwise, the minimum α may not be optimal and the optimal α can be numerically found

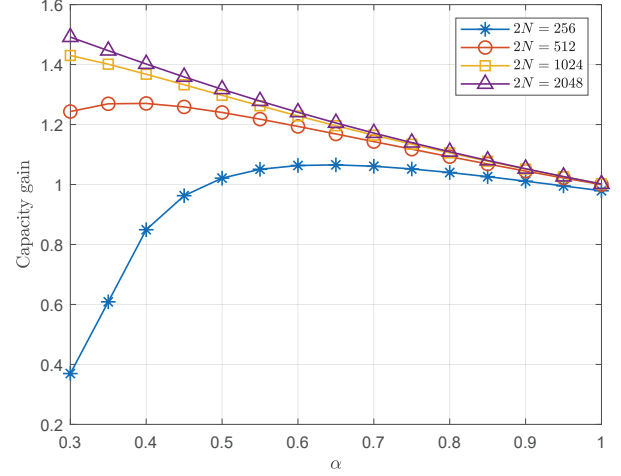


Fig. 5. The capacity gain of SISO ZIMS-VFD over conventional SISO OFDM-HD with different values of α and $2N$.

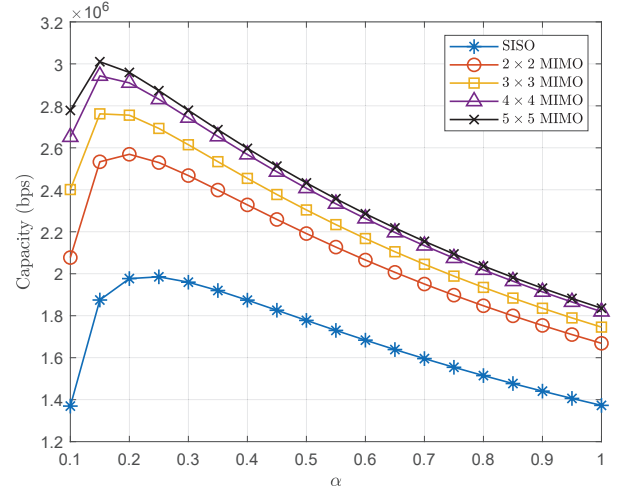


Fig. 6. The capacity ZIMS-VFD with different numbers of transmit antennas and receive antennas.

with one-dimensional search methods. Moreover, similar to Fig. 3, we can see that the capacity in Fig. 5 is approximately equal to 1 due to the relatively long zero-interval.

Figure 6 compares the capacities of SISO ZIMS-VFD, 2×2 MIMO ZIMS-VFD, 3×3 MIMO ZIMS-VFD, 4×4 MIMO ZIMS-VFD, and 5×5 MIMO ZIMS-VFD. The number of subcarriers is set to $2N = 1024$ and the power constraint for each transceiver is 40 dBm, which is averagely allocated for subcarriers. We set the range of α is from 0.1 to 1. It can be known from Fig. 6 that the capacity monotonically increases as the numbers of transmit antennas and receive antennas increase. This is because of the increase in parallel subchannels. However, we can observe that if the subcarrier number is relatively large, the increase in the number of antennas has limited impact on the capacity. In this case, increasing transmit power is more effective than increasing the number of antennas.

Figure 7 shows the average BER of ZIMS-VFD, where

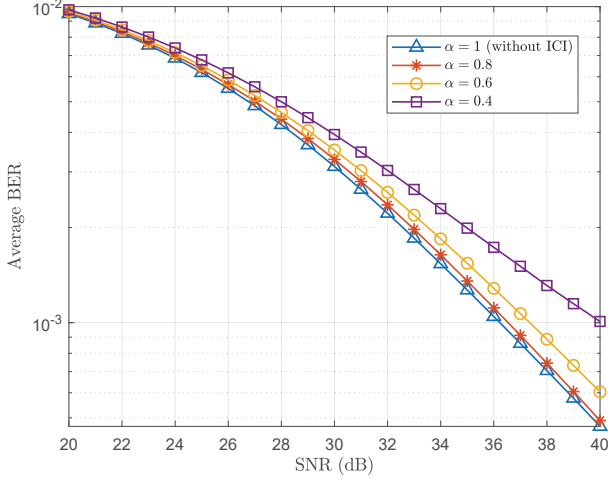


Fig. 7. Average BER of ZIMS-VFD.

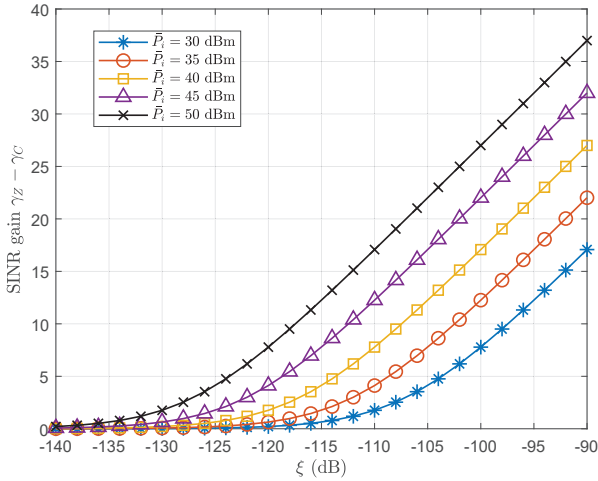


Fig. 8. The SINR gain of ZIMS-VFD over conventional FD with different values of SIC capability and \bar{P}_i .

$2N = 1024$, $K_{T,i} = K_{R,i} = 2$, the modulation scheme is QPSK, the values of α are 1, 0.8, 0.6, 0.4, and the SNR, whose expression is $\bar{P}_i/(N_0B)$, ranges from 20 dB to 40 dB. Also, MMSE detection is used for ZIMS-VFD to restore the desired symbols. If $\alpha = 1$, there are no inter-carrier interferences (ICI) since the samples are uniformly distributed in the entire OFDM period and the desired symbols are restored with DFT. We can observe from Fig. 7 that the average BER increases as the value of α decreases, which implies that the error performance decreases as the symbol rate increases. It can also be observed that if the SNR is relatively low, the average BERs corresponding to $\alpha = 0.8$, $\alpha = 0.6$, and $\alpha = 0.4$ are very close to that corresponding to $\alpha = 1$. If the SNR is relatively high, the average BERs corresponding to $\alpha = 0.8$, $\alpha = 0.6$, and $\alpha = 0.4$ do not increase much as compared to that of $\alpha = 1$. Thus, the error performance of ZIMS-VFD is not much different from the case without ICI and is acceptable in practical communication systems.

Figure 8 shows the SINR gain of ZIMS-VFD over conventional FD with SIC, which is equal to $\gamma_Z - \gamma_C$, where γ_Z is the SNR (in dB) of ZIMS-VFD and γ_C is the SINR (in dB) of conventional FD with SIC. In this paper, conventional FD with SIC refers to the FD system where the residual SI follows Gaussian distribution and its power is proportional to its transmit power. This model has been considered as a reasonable approximation in a number of existing works [31], [32]. In this evaluation, we consider the BER performance of U_1 . The expression of γ_Z is

$$\gamma_Z = \frac{\sum_{k=1}^{4N} P_2^k \lambda_1^{\tilde{k},m}}{4N\sigma_0^2}. \quad (41)$$

Based on the residual SI model, the expression of γ_C can be given by

$$\gamma_C = \frac{\sum_{k=1}^{4N} P_2^k \tilde{H}_{2,1}^{\tilde{k}}}{4N\sigma_0^2 + \sum_{k=1}^{4N} \xi P_1^k}. \quad (42)$$

where $\tilde{H}_{2,1}^{\tilde{k}}$ is the channel gain of the \tilde{k} -th subchannel and ξ ($0 \leq \xi \leq 1$) is a parameter to characterize the SIC capability. If $\xi = 0$, the SI can be perfectly canceled. If $\xi = 1$, the SIC technique is invalid. The number of subcarriers is set to $2N = 1024$. The number of transmit antennas and receive antennas are set to $K_{T,i} = K_{R,i} = 2$. The power constraint for each transceiver is set to $\bar{P}_i = 30$ dBm, $\bar{P}_i = 35$ dBm, $\bar{P}_i = 40$ dBm, $\bar{P}_i = 45$ dBm, and $\bar{P}_i = 50$ dBm, which are averagely allocated to subchannels. It can be observed that the SINR gain increases as the value of ξ increases, which implies that as compared with conventional FD with SIC, ZIMS-VFD has the better SINR performance if the SIC capability of conventional FD is relatively low. For example, if $\xi = -90$ dB and $\bar{P}_i = 50$ dBm, the SINR gain of ZIMS-VFD over conventional FD with SIC is more than 35 dB. If the SIC capability of conventional FD is relatively high, for example, $\xi = -140$ dB, it has the similar performance with ZIMS-VFD. Also, we can see that the SINR gain increases as the value of \bar{P}_i increases. This is because the residual SI power of conventional FD increases as the value of \bar{P}_i increases, but ZIMS-VFD can avoid SI by sampling the receive signal in the SI-free intervals.

Figure 9 shows the capacity gain of ZIMS-VFD over conventional FD with SIC, which refers to the ratio of the capacity of ZIMS-VFD to the capacity of conventional FD with SIC, under different values of ξ and \bar{P}_i . The parameter settings are the same as those in Fig. 8. It can be observed that the capacity gain increases as the value of ξ increases, which implies that if the SIC capability of conventional FD is relatively weak, the capacity gain of ZIMS-VFD over conventional FD with SIC is relative large. For example, if $\xi = -110$ dB and $\bar{P}_i = 50$ dBm, the capacity gain of ZIMS-VFD over conventional FD with SIC is more than 2. If the SIC capability of conventional FD is relatively strong, for example, $\xi = -130$ dB, it has the better performance than ZIMS-VFD. Also, since ZIMS-VFD can avoid SI instead of directly canceling SI in a certain proportion, the capacity gain increases as the value of \bar{P}_i increases.

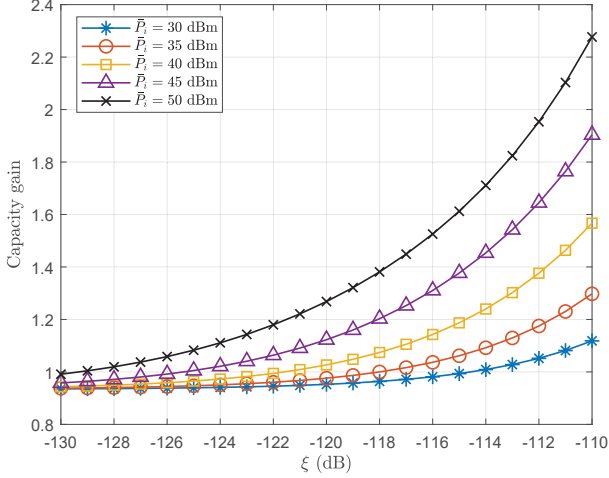


Fig. 9. The capacity gain of ZIMS-VFD over conventional FD with SIC under different values of ξ and \bar{P}_i .

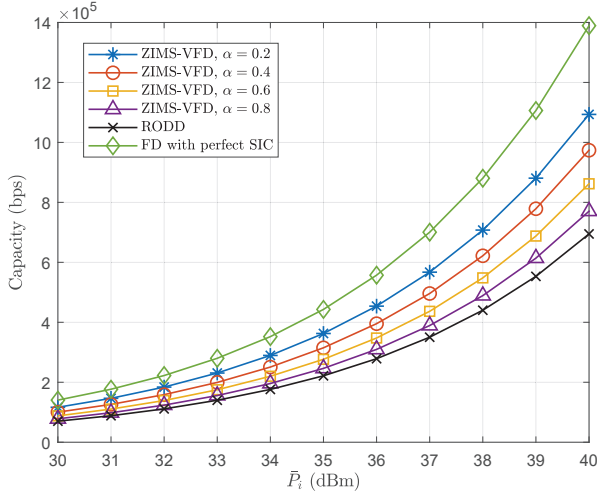


Fig. 10. The capacities of ZIMS-VFD, FD with perfect SIC, and RODD.

Figure 10 compares the capacities of ZIMS-VFD, FD with perfect SIC, and RODD, where the subcarrier number is set to $2N = 1024$, the number of transmit antennas and receive antennas are set to $K_{T,i} = K_{R,i} = 2$. To maximize the throughput of RODD, the duty cycle of RODD is set to $1/2$ and the coding rate of Vandermonde Reed Solomon codes is set to $1/2$ [23]. It can be known from Fig. 10 that the capacity of ZIMS-VFD is always lower than that of FD with perfect SIC and always higher than that of RODD. If the length of zero-interval and the transmit power are relatively small, for example, $\alpha = 0.2$ and $\bar{P}_i = 30$ dBm, ZIMS-VFD is close to FD with perfect SIC. Also, with a given α , we can see that the difference between ZIMS-VFD and FD with perfect SIC increases as the transmit power increases.

VI. CONCLUSION

In this paper, we proposed a novel FD communication technique, ZIMS-VFD, where two HD transceivers can simultane-

ously transmit signals to each other and each transceiver can effectively restore the desired symbols. The SIC techniques in the propagation domain and analog domain can be reduced. Based on OFDM, the transmission mechanism of ZIMS-VFD was introduced. We designed the transmit signal structure and determined the candidate interval, where both the SI and transitions are zero and the desired signal is within the data-interval. We have derived the condition that the candidate interval is always larger than zero. Also, we showed that the receive signal can be sampled in candidate intervals to restore the desired symbols. Numerical results verified our theoretical analyses and showed that ZIMS-VFD can effectively avoid SI and increase the capacity.

APPENDIX A PROOF FOR THEOREM 1

It can be calculated from (16) and (17) that the possible vales of $T_{C,1}^m$ are $T_Z - 2\delta + \tau_{1,1}^{\min} - \tau_{1,1}^{\max}$, $T_D + \tau_{1,1}^{\min} - \tau_{2,1}^{\min}$, $T_Z - 2\delta + \tau_{2,1}^{\max} - \tau_{1,1}^{\max}$, and $T_D + \tau_{2,1}^{\max} - \tau_{2,1}^{\min}$. Due to (5), we have $T_D + \tau_{1,1}^{\min} - \tau_{2,1}^{\min} > 0$ and $T_D + \tau_{2,1}^{\max} - \tau_{2,1}^{\min} > 0$. To guarantee $T_{C,1}^m > 0$, T_Z needs to satisfy

$$T_Z > 2\delta - \tau_{1,1}^{\min} + \tau_{1,1}^{\max} \quad (43)$$

and

$$T_Z > 2\delta - \tau_{2,1}^{\max} + \tau_{1,1}^{\max}. \quad (44)$$

On the other hand, based on (18) and (19), the possible vales of $T_{C,2}^m$ are $T_Z - 2\delta + \tau_{2,2}^{\min} - \tau_{2,2}^{\max}$, $T_Z - 2\delta + \tau_{2,2}^{\min} - \tau_{1,2}^{\min}$, $T_D + \tau_{1,2}^{\max} - \tau_{2,2}^{\max}$, and $T_D + \tau_{1,2}^{\max} - \tau_{1,2}^{\min}$. Due to (5), we have $T_D + \tau_{1,2}^{\max} - \tau_{2,2}^{\max} > 0$ and $T_D + \tau_{1,2}^{\max} - \tau_{1,2}^{\min} > 0$. To guarantee $T_{C,2}^m > 0$, T_Z needs to satisfy

$$T_Z > 2\delta - \tau_{2,2}^{\min} + \tau_{2,2}^{\max} \quad (45)$$

and

$$T_Z > 2\delta - \tau_{2,2}^{\min} + \tau_{1,2}^{\min}. \quad (46)$$

Since the difference between any two delays is less than τ_{\max} , if (20) is satisfied, (43)-(46) hold and all possible values of $T_{C,i}^m$ are always larger than 0. Thus, Theorem 1 follows.

APPENDIX B PROOF FOR THEOREM 2

We can write $\mathbf{V}_{i,m}$ as (48), which is at the top of the next page. We can observe from (48) that $\mathbf{V}_{i,m}$ is the product of a diagonal matrix, whose rank is G , and a Vandermonde matrix, whose rank is $2N$. Thus, we have $\text{Rank}(\mathbf{V}_{i,m}) \leq \min\{G, 2N\} = 2N$. Also, according to Sylvester's inequality, we have $\text{Rank}(\mathbf{V}_{i,m}) \geq G + 2N - G = 2N$. Therefore, $\text{Rank}(\mathbf{V}_{i,m}) = 2N$. Furthermore, since $\text{Rank}(\mathbf{H}_{3-i,i}) = 2N$, following the similar steps we can conclude that $\text{Rank}(\mathbf{V}_{i,m}\mathbf{H}_{3-i,i}) = 2N$. Theorem 2 follows.

$$\mathbf{V}_{i,m} = \begin{bmatrix} e^{j2\pi f_{-N+1} t_i^{1,m}} & & & \\ & \ddots & & \\ & & \ddots & \\ & & & e^{j2\pi f_{-N+1} t_i^{G,m}} \end{bmatrix} \times \begin{bmatrix} 1 & e^{j2\pi \Delta f t_i^{1,m}} & \dots & (e^{j2\pi \Delta f t_i^{1,m}})^{2N} \\ 1 & e^{j2\pi \Delta f t_i^{2,m}} & \dots & (e^{j2\pi \Delta f t_i^{2,m}})^{2N} \\ \vdots & \vdots & \ddots & \vdots \\ 1 & e^{j2\pi \Delta f t_i^{G,m}} & \dots & (e^{j2\pi \Delta f t_i^{G,m}})^{2N} \end{bmatrix}. \quad (48)$$

APPENDIX C

PROOF FOR THEOREM 3

We can write $\mathbf{V}_{i,m}^{\text{MIMO}}$ as

$$\mathbf{V}_{i,m}^{\text{MIMO}} = \begin{bmatrix} \mathbf{V}_{i,m} & & \\ & \ddots & \\ & & \mathbf{V}_{i,m} \end{bmatrix} \mathbf{H}_{3-i,i}^{\text{MIMO}}. \quad (47)$$

It can be observed that $\mathbf{V}_{i,m}^{\text{MIMO}}$ is the product of a block diagonal matrix, whose rank is $2NK_{R,i}$, and $\mathbf{H}_{3-i,i}^{\text{MIMO}}$. Thus, we have $\text{Rank}(\mathbf{V}_{i,m}^{\text{MIMO}}) \leq \text{Rank}(\mathbf{H}_{3-i,i}^{\text{MIMO}})$. In addition, according to Sylvester's inequality, we have $\text{Rank}(\mathbf{V}_{i,m}^{\text{MIMO}}) \geq 2NK_{R,i} + \text{Rank}(\mathbf{H}_{3-i,i}^{\text{MIMO}}) - 2NK_{R,i} = \text{Rank}(\mathbf{H}_{3-i,i}^{\text{MIMO}})$. Based on above analyses, we can conclude that $\text{Rank}(\mathbf{V}_{i,m}^{\text{MIMO}}) = \text{Rank}(\mathbf{H}_{3-i,i}^{\text{MIMO}})$. Theorem 3 follows.

REFERENCES

- [1] R. Askar, J. Chung, Z. Guo, H. Ko, W. Keusgen, and T. Haustein, "Interference handling challenges toward full duplex evolution in 5G and beyond cellular networks," *IEEE Wireless Communications*, vol. 28, no. 1, pp. 51–59, 2021.
- [2] K. E. Kolodziej, B. T. Perry, and J. S. Herd, "In-band full-duplex technology: Techniques and systems survey," *IEEE Transactions on Microwave Theory and Techniques*, vol. 67, no. 7, pp. 3025–3041, 2019.
- [3] N. Hu, S. Xiao, W. Pan, Q. Xu, S. Shao, and Y. Tang, "Performance analysis of the nonlinear self-interference cancellation for full-duplex communications," *Science China Information Sciences*, vol. 65, no. 11, pp. 212301, 2022.
- [4] X. Zhang, W. Cheng, and H. Zhang, "Full-duplex transmission in PHY and MAC layers for 5G mobile wireless networks," *IEEE Wireless Communications*, vol. 22, no. 5, pp. 112–121, 2015.
- [5] Z. Wan, Q. Pan, J. Li, P. Zhu, and D. Wang, "Performance analysis of full-duplex densely distributed MIMO with wireless backhaul," *Science China Information Sciences*, vol. 66, no. 6, pp. 162303, 2023.
- [6] A. Sabharwal, P. Schniter, D. Guo, D. Bliss, S. Rangarajan, and R. Wichman, "In-band full-duplex wireless: Challenges and opportunities," *IEEE Journal on Selected Areas in Communications*, vol. 32, no. 9, pp. 1637–1652, 2014.
- [7] J. Choi, M. Jain, R. Srinivasan, P. Levis, and P. Katti, "Achieving single channel, full duplex wireless communication," in *Proc. 16th ACM MOBICOM*, 2010, pp. 1–12.
- [8] M. Heino, D. Korpi, T. Huusari, E. Antonio-Rodriguez, S. Venkatasubramanian, T. Riihonen, L. Anttila, C. Icheln, K. Haneda, R. Wichman, and M. Valkama, "Recent advances in antenna design and interference cancellation algorithms for in-band full duplex relays," *IEEE Communications Magazine*, vol. 53, no. 5, pp. 91–101, 2015.
- [9] L. Laughlin, M. A. Beach, K. A. Morris, and J. L. Haine, "Electrical balance duplexing for small form factor realization of in-band full duplex," *IEEE Communications Magazine*, vol. 53, no. 5, pp. 102–110, 2015.
- [10] K. E. Kolodziej, J. G. McMichael, and B. T. Perry, "Multitap RF canceller for in-band full-duplex wireless communications," *IEEE Transactions on Wireless Communications*, vol. 15, no. 6, pp. 4321–4334, 2016.
- [11] L. Zhang, M. Ma, and B. Jiao, "Design and implementation of adaptive multi-tap analog interference canceller," *IEEE Transactions on Wireless Communications*, vol. 18, no. 3, pp. 1698–1706, 2019.
- [12] S. Ayati, A. Alizadeh, and S. Kiaei, "CMOS full-duplex mixer-first receiver with adaptive self-interference cancellation," *IEEE Transactions on Circuits and Systems I: Regular Papers*, vol. 68, no. 2, pp. 868–878, 2021.
- [13] D. Korpi, J. Tamminen, M. Turunen, T. Huusari, Y. Choi, L. Anttila, S. Talwar, and M. Valkama, "Full-duplex mobile device: pushing the limits," *IEEE Communications Magazine*, vol. 54, no. 9, pp. 80–87, 2016.
- [14] W. Cheng, X. Zhang, and H. Zhang, "Optimal dynamic power control for full-duplex bidirectional-channel based wireless networks," in *2013 Proceedings IEEE INFOCOM*, 2013, pp. 3120–3128.
- [15] E. Ahmed and A. Eltawil, "All-digital self-interference cancellation technique for full-duplex systems," *IEEE Transactions on Wireless Communications*, vol. 14, no. 7, pp. 3519–3532, 2015.
- [16] L. Zhang and H. Krishnaswamy, "Arbitrary analog/RF spatial filtering for digital MIMO receiver arrays," *IEEE Journal of Solid-State Circuits*, vol. 52, no. 12, pp. 3392–3404, 2017.
- [17] D. Korpi, L. Anttila, V. Syrjälä, and M. Valkama, "Widely linear digital self-interference cancellation in direct-conversion full-duplex transceiver," *IEEE Journal on Selected Areas in Communications*, vol. 32, no. 9, pp. 1674–1687, 2014.
- [18] Q. Li, M. Yu, A. Pandharipande, X. Ge, J. Zhang, and J. Zhang, "Performance of virtual full-duplex relaying on cooperative multi-path relay channels," *IEEE Transactions on Wireless Communications*, vol. 15, no. 5, pp. 3628–3642, 2016.
- [19] I. Orikumhi, C. Y. Leow, and Z. Ding, "Wireless information and power transfer in MIMO virtual full-duplex relaying system," *IEEE Transactions on Vehicular Technology*, vol. 66, no. 12, pp. 11001–11010, 2017.
- [20] Y.B. Kim, K. Yamazaki, and B. C. Jung, "Virtual full-duplex cooperative NOMA: Relay selection and interference cancellation," *IEEE Transactions on Wireless Communications*, vol. 18, no. 12, pp. 5882–5893, 2019.
- [21] D. Guo and L. Zhang, "Virtual full-duplex wireless communication via rapid on-off-division duplex," in *2010 48th Annual Allerton Conference on Communication, Control, and Computing (Allerton)*, 2010, pp. 412–419.
- [22] L. Zhang and D. Guo, "Virtual full duplex wireless broadcasting via compressed sensing," *IEEE/ACM Transactions on Networking*, vol. 22, no. 5, pp. 1659–1671, 2014.
- [23] Z. Tong, C. Russ, S. Vanka, and M. Haenggi, "Prototype of virtual full duplex via rapid on-off-division duplex," *IEEE Transactions on Communications*, vol. 63, no. 10, pp. 3829–3841, 2015.
- [24] D. Tse and P. Viswanath, *Fundamentals of Wireless Communications*, Cambridge University Press, 2005.
- [25] J. Proakis and M. Salehi, *Digital Communications*, McGraw-Hill Companies, Inc., 2005.
- [26] Y. Cho, J. Kim, W. Yang, and C. Kang, *MIMO-OFDM Wireless Communications With MATLAB*, John Wiley & Sons, Inc., 2010.
- [27] A. Goldsmith, *Wireless Communications*, Cambridge University Press, 2005.
- [28] E. Chong and S. Žak, *An Introduction to Optimization*, John Wiley & Sons, Inc., 2013.
- [29] L. Yuan, Z. Wang, W. Wei, and X. Han, "High-frequency broadband rf transmit-receive switch for pulsed magnetic field NMR," *IEEE Transactions on Instrumentation and Measurement*, vol. 72, pp. 1–9, 2023.
- [30] Mohamed A. Abou-Khousa and Ademola A. Mustapha, "Wideband rf transmit-receive switch for multi-nuclei nmr spectrometers," *IEEE Transactions on Circuits and Systems II: Express Briefs*, vol. 69, no. 3, pp. 904–908, 2022.
- [31] A. Cirik, Y. Rong, and Y. Hua, "Achievable rates of full-duplex MIMO radios in fast fading channels with imperfect channel estimation," *IEEE Transactions on Signal Processing*, vol. 62, no. 15, pp. 3874–3886, 2014.
- [32] X. Xu, X. Chen, M. Zhao, S. Zhou, C. Chi, and J. Wang, "Power-efficient distributed beamforming for full-duplex MIMO relaying networks," *IEEE Transactions on Vehicular Technology*, vol. 66, no. 2, pp. 1087–1103, 2017.